Electronic supplementary information to: "Crucial impact of layer exchange on temperature programmed desorption"

Tobias Dickbreder, Ralf Bechstein and Angelika Kühnle

Contents

1 Introduction

In our manuscript we present a kinetic model to describe desorption in systems with two layers and exchange between those layers. This model shows that considering layer exchange can alter the desorption spectrum considerably even for second layer coverages as small as 1×10^{-6} ML. We identify a second-layer desorption mechanism where particles in the first layer *hop on top* of other particles prior to desorption. Moreover, we show that the desorption *via* this *hop on top* mechanism results in a modified Polanyi-Wigner equation given that layer exchange is in quasi-equilibrium and the energy difference between the layers is sufficiently high. Our study thus demonstrates that considering layer exchange can make transient desorption positions relevant even for coverages where the vast majority of particles resides in the first layer.

In this ESI, we provide additional information on our model and on the simulation of desorption spectra based on our model. To this end, we discuss in detail which cases are relevant for the relation between the rates of layer exchange and desorption and how the these cases can be characterized in terms of kinetic parameters. We use this characterization to develop a simple way to classify a given set of kinetic parameters. Moreover, we present how our model can be adapted to another geometry and compare the results to the simple chain geometry discussed in our manuscript. We elucidate the influence of the initial coverage on the contribution of desorption *via hop on top* on the desorption spectrum. Last, we explain technical aspects concerning the numerical calculation of desorption spectra from the model differential equations.

2 Relevant Cases

In our manuscript we introduce the three cases in terms of the relation between the rates of desorption and layer exchange (Fig. S1). Namely, we investigate (a) kinetically-hindered layer exchange, (b) balance between layer exchange and desorption, and (c) quasi-equilibrium layer exchange. In case (a), kinetically-hindered layer exchange, layer exchange is considerably slower than desorption thus, layer exchange does not take place on the timescale of desorption. This corresponds to a significantly higher energy barrier for layer exchange than for desorption as presented in Fig. S1 (a). In case (b) the rates of layer exchange and desorption are of the same order in both layers, which is why the kinetics of desorption are governed by a balance between layer exchange and desorption. In terms of Gibbs free energy this means that $\Delta G_{\mathrm{d},2} \approx \Delta G_{\mathrm{le},2\to1}$ (see Fig. S1 (b)). Case (c) is characterised by significantly faster layer exchange than desorption, *i.e.*, a significantly higher energy barrier for desorption than layer exchange (see Fig. S1 (c)). Hence, layer exchange is in a state of quasi-equilibrium on the timescale of desorption.

In this section, we discuss a quantitative classification of the three cases and provide a simple method to assign a case to a given set of kinetic parameters. Moreover, we present additional simulated desorption spectra for the cases of kinetically-hindered layer exchange (case (a)) and balance between layer exchange and desorption (case (b)).

Desorption spectra shown in this section are calculated numerically as described in section 6. In order to do so, we use the same kinetic parameters we use in for the simulations in our manuscript (see Tab. 1). In addition to these kinetic parameters the simulations for cases (a) and (b) require activation barriers for layer exchange $\Delta E_{\mathrm{le},2\to1}$ and $\Delta S_{\mathrm{le},2\to1}$. Those barriers are specified in the corresponding sections. Moreover, it is necessary to set the initial coverages in the first and second layer for a given initial total coverage. These coverages were obtained from the total coverage with a simple ballistic model described in section 6.1. Briefly, this model is based on the assumption that the particles hit the surface randomly while dosing. When a particle hits an unoccupied adsorption

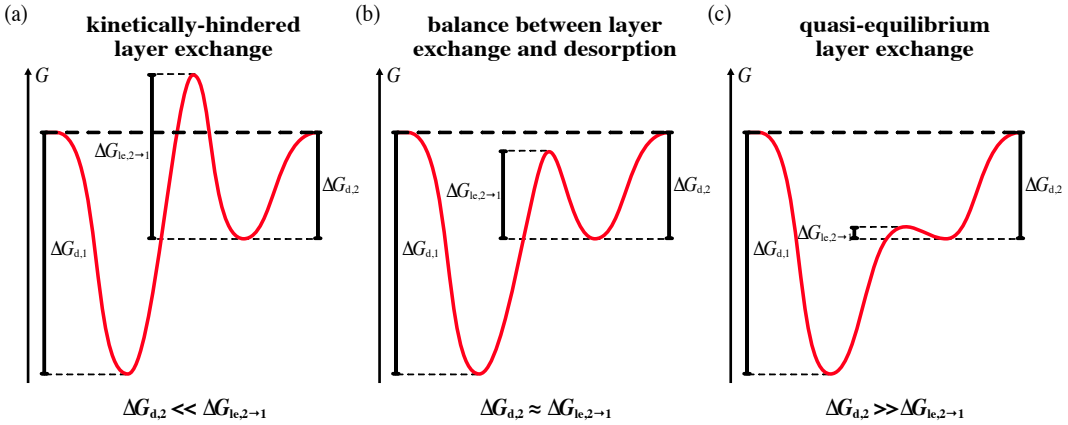

Figure S1: Schematic Gibbs free energy diagrams for the three cases discussed here, which are kinetically-hindered layer-exchange (a), balance between layer exchange and desorption (b) and quasi-equilibrium layer exchange (c). In this scheme the Gibbs free energy landscape is characterised by the barriers for desorption from the first and second layer $\Delta G_{\mathrm{d},1}$ and $\Delta G_{\mathrm{d},2}$ respectively, and the barrier for layer exchange from the second to the first layer $\Delta G_{\mathrm{le},2\to1}$.

site it sticks with a given probability and is otherwise rejected. Particles colliding with an occupied adsorption site do not adsorb.

Table 1: Kinetic energy barriers ΔE_{x} and entropy changes ΔS_{x} of desorption from the first (d,1) and second layer (d,2) used for the simulation of desorption spectra.

Process	ΔE_{x} / eV	ΔS_{x} / k_{B}
d,1	1.0	10
d,2	0.5	2

2.1 Case classification and stability

In Fig. S1, we considered rather extreme examples, which clearly correspond to one of the three cases. For sets of kinetic parameters in the intermediate range between two cases, however, an intuitive classification might fail. Therefore, we discuss in detail how different kinetic parameters correspond to the three cases discussed above. To this end, we determine which conditions are necessary for the rates of layer exchange and desorption to be equal in the first and second layer and how to express these conditions with the energy barriers of the system.

First layer In the first layer, we compare the rate of layer exchange $\frac{r_{\mathrm{le},1\to2}}{N_{\mathrm{ad}}}$ from the first to the second layer with the first-layer desorption rate $\frac{r_{\mathrm{d},1}}{N_{\mathrm{ad}}}$. Those rates are identical if Eq. 1 holds true.

$$2k_{\mathrm{le},1\to2}(\theta_1-\theta_2)^2 = k_{\mathrm{d},1}(\theta_1-\theta_2) \tag{1}$$

Eq. 1 can be rearranged to Eq. 2.

$$\frac{k_{\mathrm{d},1}}{k_{\mathrm{le},1\to 2}} = 2(\theta_1 - \theta_2) \tag{2}$$

When we apply transition state theory for the rate constants and $\Delta G_{\mathrm{x}} = \Delta E_{\mathrm{x}} - T\Delta S_{\mathrm{x}}$ we obtain Eq. 3. Additionally, we use the relation between the rate constants of layer exchange and desorption derived in the main text ($k_{\mathrm{d},1}/k_{\mathrm{d},2} = k_{\mathrm{le},1\to 2}/k_{\mathrm{le},2\to 1}$).

$$\Delta G_{\mathrm{le},2\to 1} - \Delta G_{\mathrm{d},2} = k_{\mathrm{B}}T\left[\ln(2) + \ln(\theta_1 - \theta_2)\right] \tag{3}$$

Second layer When we apply the same strategy as shown for the first layer, we obtain for the second layer Eq. 4 and Eq. 5.

$$2k_{\mathrm{le},2\to 1}(1-\theta_1)\theta_2 = k_{\mathrm{d},2}\theta_2 \tag{4}$$

$$\Delta G_{\mathrm{le},2\to 1} - \Delta G_{\mathrm{d},2} << k_{\mathrm{B}}T\left[\ln(2) + \ln(1 - \theta_1)\right] \tag{5}$$

We can use these equal-rate-equations for the first and second layer (Eq. 3 and Eq. 5) in order to determine which case applies for a given set of kinetic parameters and temperature. To this end, Fig. 4 shows $\frac{\Delta G_{\mathrm{le},2\to 1} - \Delta G_{\mathrm{d},2}}{k_{\mathrm{B}}T}$ as a function of the first- and second-layer coverages, where the surface of equal rates in the first (second) layer is displayed in red (blue). For a specific set of kinetic parameters the same quantity ($\frac{\Delta G_{\mathrm{le},2\to 1} - \Delta G_{\mathrm{d},2}}{k_{\mathrm{B}}T}$) can be calculated and is displayed in Fig. S2 as a black plane for an example of case (c) (specific parameters given in the figure caption). This means that the rates of desorption and layer exchange are equal at the intersection of the black plane with an equal-rate surface. Moreover, desorption is faster (slower) than layer exchange in one layer if the black plane is above (below) the corresponding equal-rate surface. The difference between the black plane and the equal rate surface is a measure for the difference in rates. Hence, Fig. S2 shows which case applies for a given set of kinetic parameters by evaluation of the difference between the equal-rate surfaces and $\frac{\Delta G_{\mathrm{le},2\to 1} - \Delta G_{\mathrm{d},2}}{k_{\mathrm{B}}T}$ along the path of a desorption spectrum in terms of T, θ_1 and θ_2. However, the evaluation of Fig. S2 along the path of a desorption spectrum requires the knowledge of this path and, thus, of the desorption spectrum. As this information is not available beforehand, we provide a simplified case stability diagram (Fig. S3) for practical purposes.

For the simplified case stability diagram, we use Fig. S2 to find critical values for the change between the cases. To ensure case (a) (case (c)) the term $\frac{\Delta G_{\mathrm{le},2\to 1} - \Delta G_{\mathrm{d},2}}{k_{\mathrm{B}}T}$ has to be larger (smaller) than 6 (-8). In the intermediate range, case (b) applies. These critical values are independent of the first- and second-layer coverages, so the only remaining variable for the desorption path is the temperature. As a consequence, we can determine the case from a plot of $\frac{\Delta G_{\mathrm{le},2\to 1} - \Delta G_{\mathrm{d},2}}{k_{\mathrm{B}}T}$ as a function of temperature as shown in Fig. 5. If $\frac{\Delta G_{\mathrm{le},2\to 1} - \Delta G_{\mathrm{d},2}}{k_{\mathrm{B}}T}$ is smaller than -8 case (c) is applicable (cyan area). If $\frac{\Delta G_{\mathrm{le},2\to 1} - \Delta G_{\mathrm{d},2}}{k_{\mathrm{B}}T}$ is between -8 and 6, the desorption spectrum is governed by case (b) and for values of $\frac{\Delta G_{\mathrm{le},2\to 1} - \Delta G_{\mathrm{d},2}}{k_{\mathrm{B}}T}$ greater than 6 we can apply case (a) (violet area).

If the case changes in the course of a TPD experiment (black curve changes region) it needs to be considered that equilibrium condition is displayed in Fig. S3, which is not necessarily reached in the experiment.

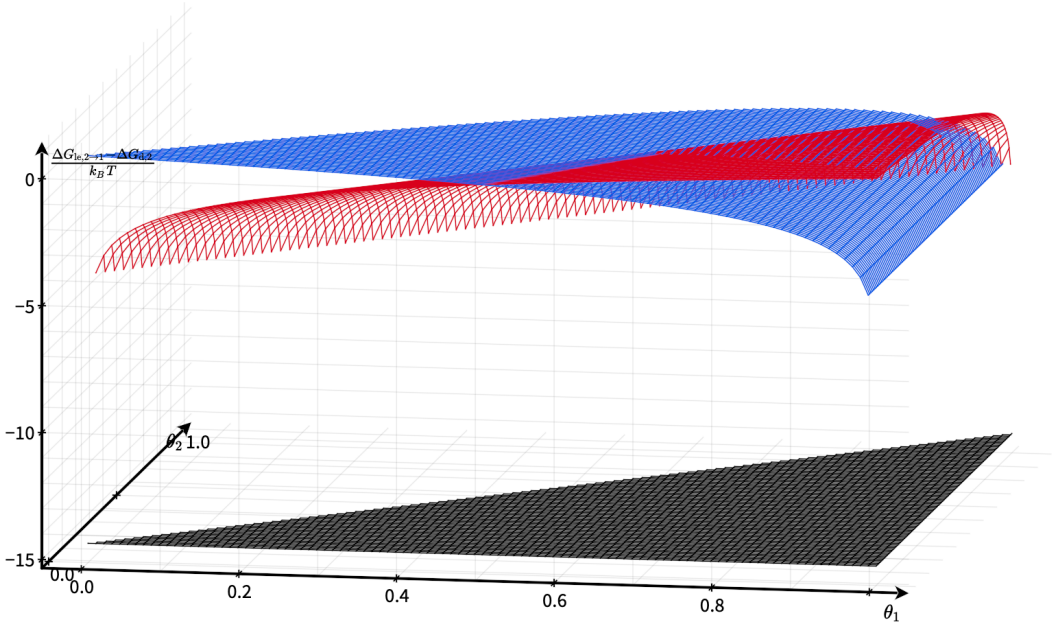

Figure S2: Difference $\frac{\Delta G_{\mathrm{le},2\to1} - \Delta G_{\mathrm{d},2}}{k_\mathrm{B} T}$ as a function of the first- and second-layer coverages. The equal-rate surfaces for the first and second layer are displayed in red and blue, respectively, and the $\frac{\Delta G_{\mathrm{le},2\to1} - \Delta G_{\mathrm{d},2}}{k_\mathrm{B} T}$ value calculated for an example of case (c) (parameters in Tab. 1, $\Delta E_{\mathrm{le},2\to1} = 0.1\,\mathrm{eV}$ and $\Delta S_{\mathrm{le},2\to1} = 0$) and a temperature of 280 K is shown as a black plane. Hence, the rates of layer exchange and desorption of the current system are equal at the intersection between the black plane and the equal-rate surfaces. If the black plane is above (below) an equal-rate surface the desorption rate is higher (smaller) than the rate of layer exchange in the corresponding layer.

2.2 Kinetically-hindered layer exchange

In case of kinetically-hindered layer exchange, desorption is much faster than layer exchange in both layers, which corresponds to a significantly higher barrier for layer exchange than for desorption (see section 2.1). Hence, desorption is the preferred process while layer exchange is negligible on the timescale of desorption. This means that particles can only diffuse within their layer or desorb, but they cannot change from the first to the second layer or the other way around. Consequently, there is no coupling between desorption from the first and second layer as long as the energy difference between the layers is high enough that all particles from the second layer desorb before desorption from the first layer gets significantly fast. In this line of argumentation, we expect that each individual peak (first-layer and second-layer desorption) can be described perfectly with a Polanyi-Wigner approach.

A typical desorption spectrum simulated for the case of kinetically-hindered layer exchange is displayed in Fig. S4. For the initial coverage 1.0 ML is chosen. Interestingly, the modelled desorption spectrum (violet) in Fig. S4 (a) shows two desorption signals — one for desorption from the first and second layer, respectively — not just one for desorption from the first layer as suggested by the total coverage of 1.0 ML. This is caused by the way particles are dosed onto the surface.

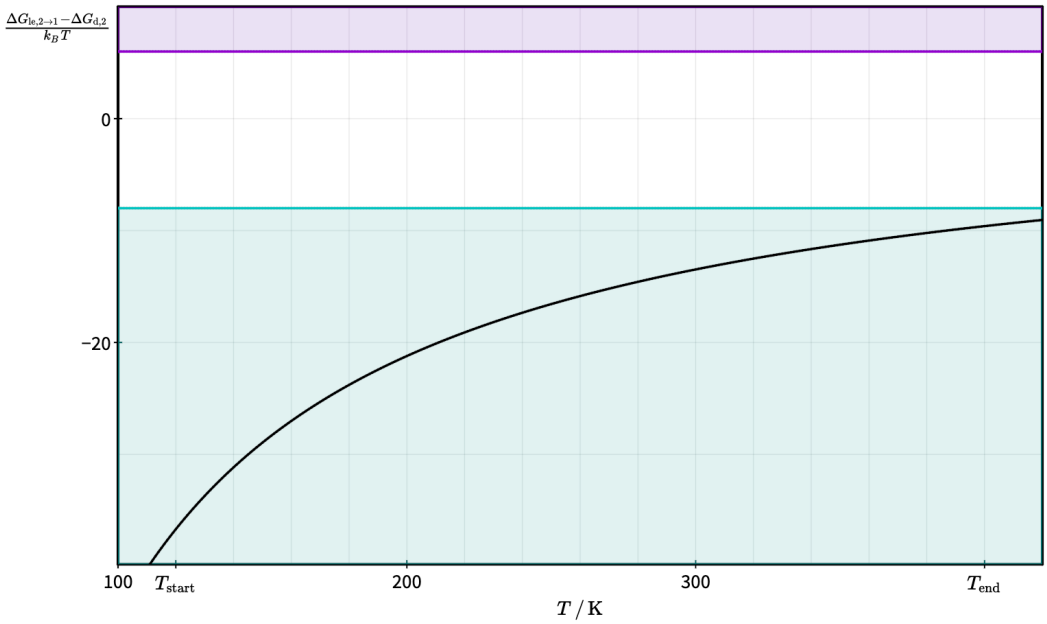

Figure S3: Simplified case stability diagram. The Gibbs free energy difference $\frac{\Delta G_{le,2\to1}-\Delta G_{d,2}}{k_B T}$ is displayed as a function of temperature for the specified kinetic parameters. Those parts of the diagram where layer exchange is kinetically-hindered (case (a)) are displayed in violet and those parts where layer exchange is in equilibrium (case (c)) in cyan. For determination of these classification areas, critical $\frac{\Delta G_{le,2\to1}-\Delta G_{d,2}}{k_B T}$ values were used as explained in the text. Moreover, the start and end temperatures of the TPD experiment (*i.e.* the relevant temperature range) are marked with tick on the temperature axis.

While dosing, the particles are not deposited in the first layer solely, but hit the surface randomly, so particles are deposited in the second layer as well as soon as there is a significant first layer occupation. As we consider a case with a high barrier for layer exchange, this barrier prevents particles from layer exchange at the temperature relevant for desorption. Certainly, the particles cannot change their layer during the dosing phase at much lower temperatures either, which is why they desorb from their initial state causing two desorption signals. This conclusion is supported by the first- (red) and second-layer (blue) coverages in Fig. S4 (b), because there is no simultaneous decrease in second-layer coverage and increase in first-layer coverage, which would be indicative for an exchange of particles from the second to the first layer.

Apart from the fact that the second layer desorption peak appears before the first layer is completely filled, the modelled desorption spectrum in Fig. S4 (a) shows two typical first-order desorption signals for desorption from the first and second layer. Both signals consist of a single desorption path each, which can be seen in Fig. S4 (a) as the contributions of first-layer (second-layer) desorption in red (blue) coincide with the total desorption spectrum in violet in the range of the second (first) desorption peak. In Fig. S4 (b) this picture is supported by the observation that the coverages of the first (second) layer are constant while desorption from the second (first) layer takes place. The differences between the first layer desorption signal and the first-order Polanyi-Wigner desorption spectrum (grey) can be explained solely by the difference between the coverage

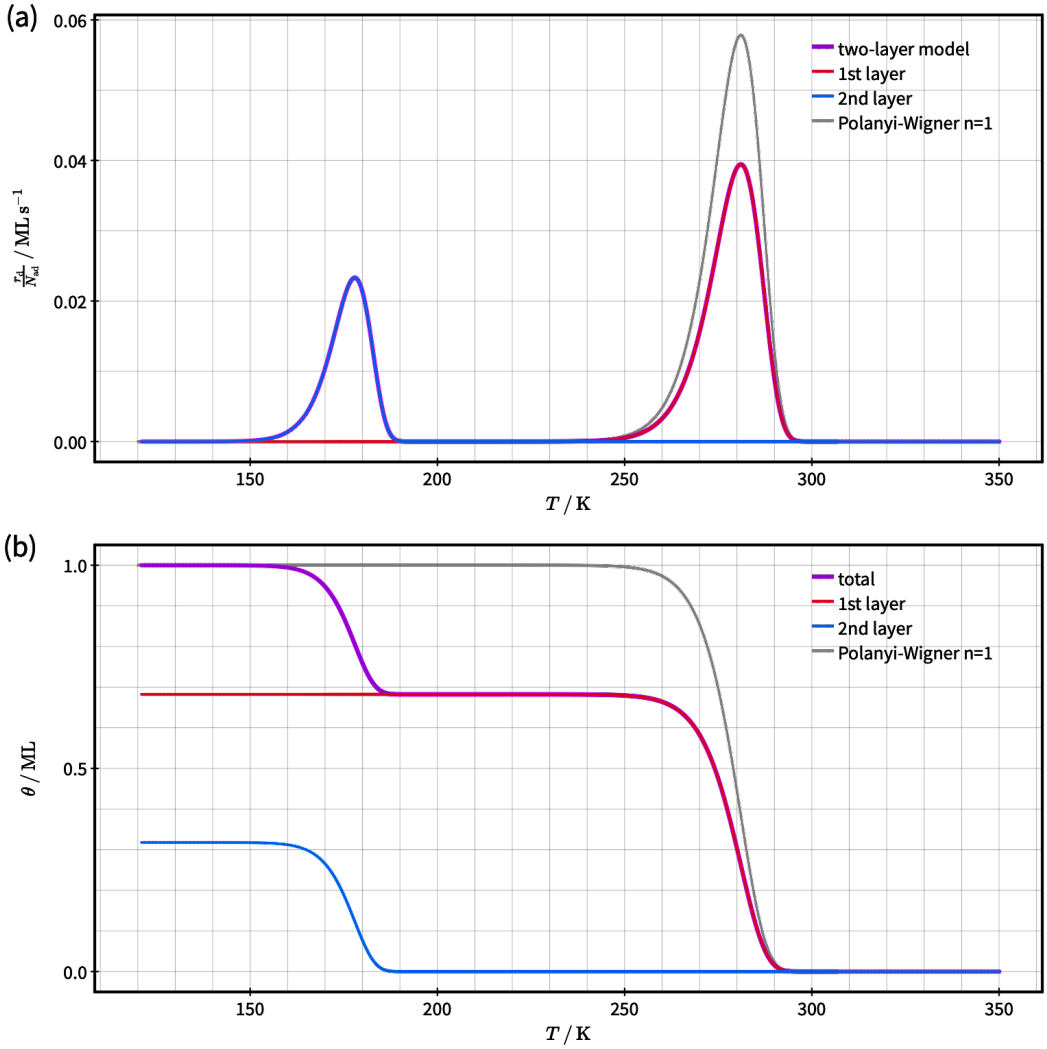

Figure S4: Comparison of simulated desorption spectra (a) and total coverage as a function temperature (b) for a two-layer system with kinetically-hindered layer exchange according to our model (violet) and a first order Polanyi-Wigner process with the same kinetic parameters as used for desorption from the first layer (grey). For the two-layer model the contributions of desorption from the first (red) and second (blue) layer are shown in (a) and the corresponding coverages in (b). The TPD data was calculated with the kinetic parameters for desorption given in the text and an additional barrier for layer exchange of $\Delta E_{\mathrm{le},2\to1} = 0.7\,\mathrm{eV}$ and $\Delta S_{\mathrm{le},2\to1} = 0\,\mathrm{k_B}$. Initial coverages for this simulation were obtained with a ballistic model.

in the first layer and the total coverage[§]. We conclude that in this case desorption from the first and

[§]For the calculation of the first-order Polanyi-Wigner desorption spectrum the initial coverage was the total coverage

second layer are independent from each other as long as the energy difference between the layers is high enough for their desorption signals not to overlap. Consequently, a Polanyi-Wigner model is perfectly suitable to describe desorption from the first and second layer respectively. Moreover, we can use analysis methods based on the Polanyi-Wigner equation — *e.g.*, leading edge or complete analysis — for the determination of kinetic parameters for desorption. However, the appearance of the second layer desorption peak before the first layer is completely filled can lead to problems with calibration. It is a common procedure to calibrate the desorption rate with the intensity of the first layer desorption spectrum just before the second layer desorption peak appears. In case of kinetically-hindered layer exchange, we cannot use this strategy as it would cause an erroneously high desorption rate. This, in turn, introduces (additional) errors in the kinetic parameters in general and especially in the entropy barrier for desorption. Instead, we can use the maximum peak intensity achievable for the first layer desorption signal to calibrate our data.

An experimental strategy to solve this problem with calibration is annealing the sample between dosing and the actual TPD measurement. If the sample is heated to an intermediate temperature prior to the TPD experiment particles in the second layer can either change to the first layer or desorb*. Thus, the first layer will be occupied first, which results in a layer-by-layer appearance of the desorption signals. In case of kinetically-hindered layer exchange, however, we need to consider that particles in the second layer will only desorb, but they do not change from the second to the first layer. Therefore, it is necessary to dose until the first layer is completely occupied, before the initial coverage can be adjusted by varying the annealing time.

The use of annealing steps in TPD experiments have been reported, *e.g.*, by Kachel et. al.[1] for naphthalene and azulene on Ag(111) and Cu(111). They have observed that TPD experiments without annealing show irregular leading edges, while the line shapes after annealing are regular and well defined. They have attributed this difference in leading edges to the formation of metastable phases during dosing, which transform or desorb when the sample is annealed. They have pointed out that these irregular leading edges can lead to erroneous results in the data analysis.[1]

2.3 Balance between layer exchange and desorption

Next, we turn to case (b), where the reaction rates of layer exchange and desorption are on the same order, *i.e.*, the corresponding energy barriers $\Delta G_{\mathrm{le},2\to1}$ and $\Delta G_{\mathrm{d},2}$ are similar (see Fig. S1 (b)). Hence, neither layer exchange nor desorption alone govern the desorption spectrum but the balance between both processes is crucial for the kinetics of desorption. This means that layer exchange takes place on the timescale of desorption, but is not fast enough to reach its equilibrium state, so we can interpret case (b) as an intermediate between the limiting cases of kinetically-hindered layer exchange (a) and quasi-equilibrium layer exchange (c). Consequently, we expect the desorption spectrum to depend on the initial coverages as the system cannot equilibrate prior to desorption.

Simulated TPD data for the case of a balance between layer exchange and desorption are presented in Fig. S5. As in case (a) (see Fig. S4) the desorption spectrum for an initial total coverage of 1.0 ML — *i.e.*, the violet curve in Fig. S5 (a) — shows two desorption signals. In this spectrum the desorption signal at lower temperatures corresponds to the desorption of particles in the second layer, whereas the second peak results from desorption of particles originating from the first

as no second layer exists for this model. For the two-layer model, however, the total coverage is distributed on both layers as described above.

*This holds true as long as the energy difference between the layers is sufficiently high. If the energy difference between the layers is indeed small, both layers are significantly occupied in thermal equilibrium. Consequently, annealing will not create a layer by layer occupation in those cases.

layer. In this case, the appearance of a second-layer desorption signal for coverages below 1.0 ML is caused by a kinetic-trapping mechanism similar to the mechanism described for case (a). Here, we can observe that the decrease in total and second-layer coverage during second-layer desorption is accompanied by an increase in first layer coverage (see Fig. S5 (b)). This means that layer exchange from the second to the first layer is not hindered during the entire TPD experiment, but is activated in the same temperature range as desorption from the second layer. Hence, some particles desorb from the second layer while others change to the first layer when the second layer becomes depopulated. Consequently, we cannot describe the second-layer desorption signal with a simple Polanyi-Wigner term as two processes —layer exchange from the second to the first layer and desorption from the second layer— are pivotal for the change in second-layer coverage.

The high-temperature desorption peak in Fig. S5 (a) shows a flatter low-temperature rise, a higher peak width and a smaller maximum desorption rate compared to the first-order desorption spectrum (grey). We can explain the smaller maximum desorption rate and total integral of the desorption signal with the fact that some molecules already desorbed from the second layer as discussed in section 2.2. The higher peak width and flatter low temperature rise are caused by desorption *via hop on top* as explained in our manuscript. However, these features are less developed than in case (c), because layer exchange is slower than in case (c) and, thus, desorption *via hop on top* occurs less frequently. Fig. S5 (a) confirms this interpretations as the contribution of second-layer desorption (blue curve) during desorption from the first layer is smaller than in case (c) (see Fig. 3 (a)).

In the interpretation of Fig. S5 (b) we discussed that second-layer desorption in case of a balance between layer exchange and desorption is governed by this balance as well. To further investigate the influence of layer exchange on the second-layer desorption signal in this case we calculated desorption spectra with varying initial coverages as shown in Fig. S6 (a) (only the second layer desorption signals are shown). Note that the initial coverages in the first and second layer were calculated with our ballistic model as explained previously. Fig. S6 (a) shows that the maximum of the second-layer desorption signal shifts to higher temperatures with increasing initial coverages (168 K to 178 K). This shift is typical for desorption kinetics with a fractional order. In this case, however, the peak shift is not caused by a fractional desorption order, but by the competition between desorption from the second layer and layer exchange from the second to the first layer. As a consequence, it is necessary to explicitly consider both layer exchange and desorption in the analysis of the second-layer desorption peak.

To elucidate whether the kinetics of desorption can be simplified by a changed experimental procedure, we consider the effect of annealing discussed in section 2.2. In order to do so, we simulate desorption spectra with an annealing step between dosing and the TPD experiment. The simulated annealing experiment works as follows: For all simulated desorption spectra we started with an initial coverage of 2.0 ML after dosing at 120 K. Next, the surface was heated to the annealing temperature of 165 K with a heat rate of 1.0 K s^{-1}, held at this temperature for varying annealing times and cooled back to 120 K. After the simulated annealing step, we simulate desorption spectra with the initial coverages after annealing as described in section 6. We present desorption spectra simulated with the described annealing procedure in Fig. S6 (b). Fig. S6 (b) shows that the shift in the peak maxima vanishes for the annealed desorption spectra and, thus, the second-layer desorption peaks can be described with simple first-order kinetics. This change in kinetics is caused by the fact that layer exchange from the second to the first layer can only take place if there are unoccupied adsorption sites in the first layer. Hence, the influence of layer exchange on the second-layer desorption signal vanishes for a completely occupied first layer. Only the contribution of second-layer desorption remains which follows first-order Polanyi-Wigner kinetics. We conclude that annealing can be used to simplify the kinetics of desorption and, thus, the analysis of desorption spectra sig-

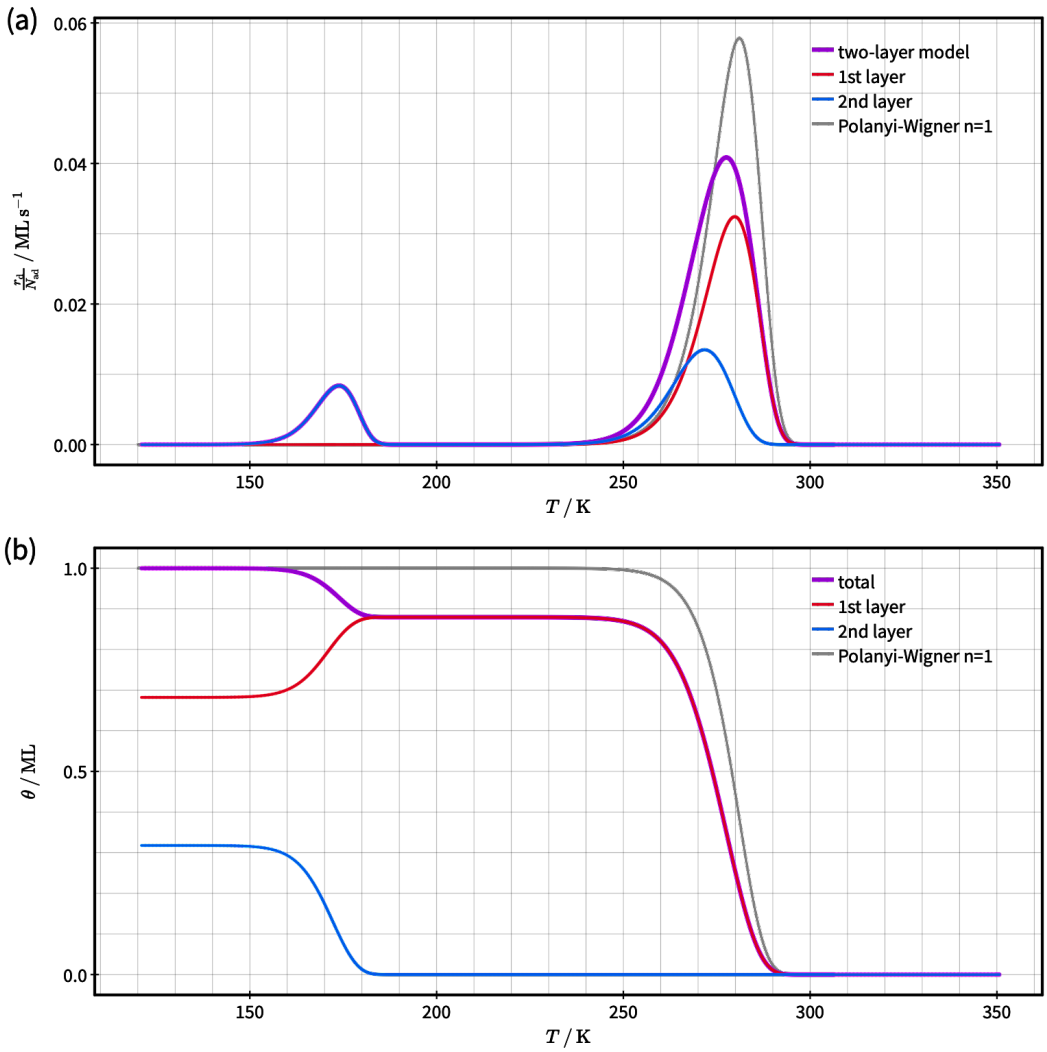

Figure S5: Comparison of simulated desorption spectra (a) and total coverage as a function temperature (b) for a two-layer system with a balance between layer exchange and desorption according to our model (violet) and a first order Polanyi-Wigner process with the same kinetic parameters as used for desorption from the first layer (grey). For the two-layer model the contributions of desorption from the first (red) and second (blue) layer are shown in (a) and the corresponding coverages in (b). The TPD data was calculated with the kinetic parameters for desorption given in the text and an additional barrier for layer exchange of $\Delta E_{\mathrm{le},2\to1} = 0.45\,\mathrm{eV}$ and $\Delta S_{\mathrm{le},2\to1} = 0\,\mathrm{k_B}$. Initial coverages for this simulation were obtained with a ballistic model.

nificantly. However, our model does not include layer exchange with the third (and higher layers), so we cannot conclude that the second-layer desorption follows first order kinetics after annealing. The first-layer desorption signals are not influenced by annealing the sample prior to desorption

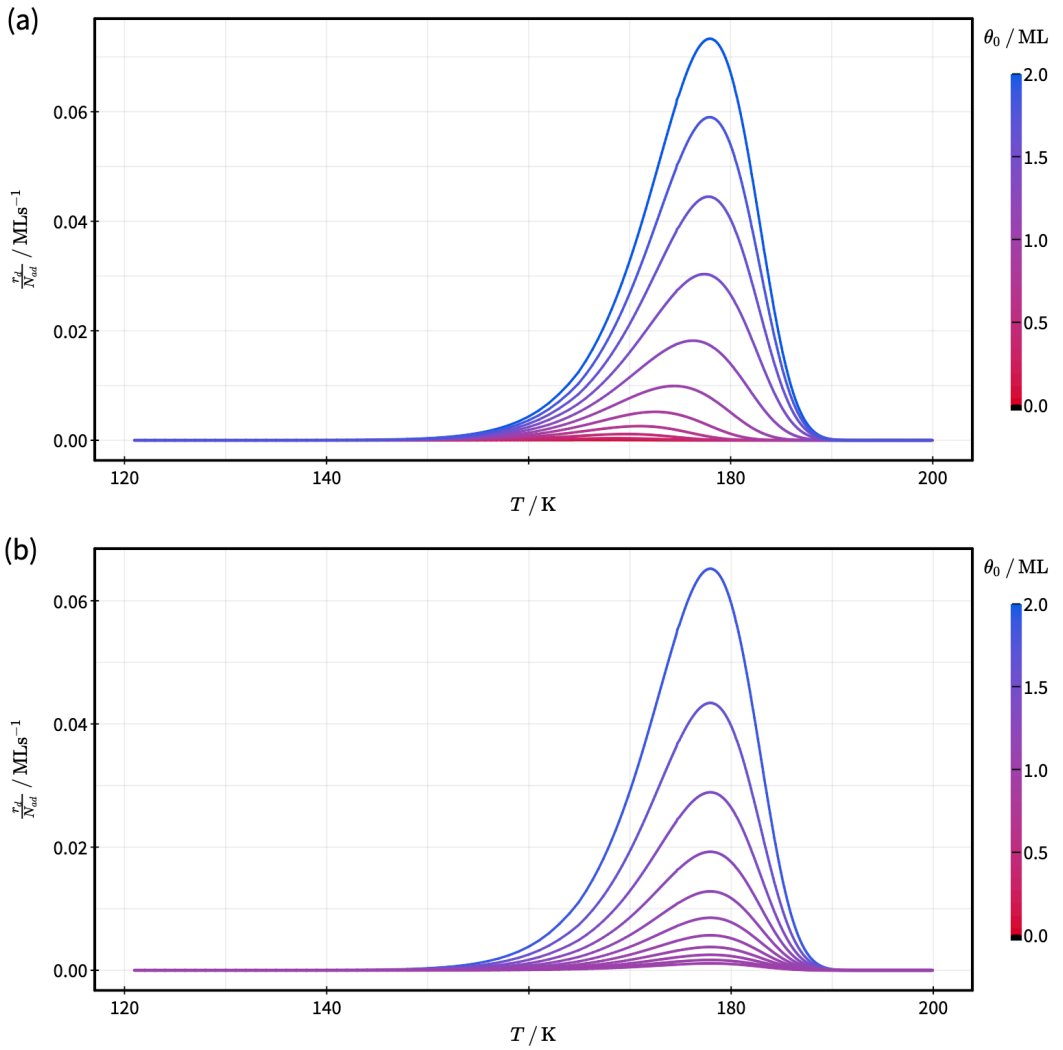

Figure S6: Comparison of simulated second-layer desorption signals in case of a balance between layer exchange for different experimental procedures. (a) Simulated second-layer desorption signals for initial coverages θ_0 of 0.1 ML, 0.3 ML, 0.5 ML, 0.7 ML, 0.9 ML, 1.1 ML, 1.3 ML, 1.5 ML, 1.7 ML and 1.9 ML. Initial coverages distributions were calculated based on a ballistic model explained in section 6.1. (b) Simulated second-layer desorption signals after annealing as explained in the text. The displayed were calculated with an initial coverage after dosing of 2.0 ML and annealing times of 0.30 s, 60 s, 90 s, 120 s, 150 s, 180 s, 210 s, 240 s, 270 s and 300 s at 265 K. TPD data in both figure part was calculated with the kinetic parameters for desorption given in the text and an additional barrier for layer exchange of $\Delta E_{\mathrm{le},2\to1} = 0.45$ eV and $\Delta S_{\mathrm{le},2\to1} = 0\,\mathrm{k_B}$.

(except for the total peak intensity, see interactive visualisation (see section 6)).

We observe this effect of layer exchange on the second-layer desorption signal solely for case (b),

because it only appears when layer exchange is activated in the same temperature range as desorption from the second layer. Consequently, the second-layer desorption peaks in case of kinetically-hindered layer exchange (case (a)) and quasi-equilibrium layer exchange (case (c)) always agree perfectly with a first-order Polanyi-Wigner approach.

3 Simple chain geometry

In our manuscript, we investigate the general influence of layer exchange on the kinetics of desorption. To this end, we develop a kinetic model for layer exchange and desorption on the example of the rather simple simple chain geometry. This results in a set of coupled differential equations for the time evolution of the first-layer and second-layer coverage (Eq. 6 and Eq. 7) as well as the desorption rate (Eq. 8). Based on these equations we derive a modified Polanyi-Wigner equation in case of a sufficiently high energy difference between the layers and quasi-equilibrium layer exchange.

$$\frac{\mathrm{d}\theta_1}{\mathrm{d}t} = -2k_{\mathrm{le},1\to2}(\theta_1-\theta_2)^2 + 2k_{\mathrm{le},2\to1}(1-\theta_1)\theta_2 - k_{\mathrm{d},1}(\theta_1-\theta_2) \tag{6}$$

$$\frac{\mathrm{d}\theta_2}{\mathrm{d}t} = 2k_{\mathrm{le},1\to2}(\theta_1-\theta_2)^2 - 2k_{\mathrm{le},2\to1}(1-\theta_1)\theta_2 - k_{\mathrm{d},2}\theta_2 \tag{7}$$

$$\frac{r_\mathrm{d}}{N_\mathrm{ad}} = k_{\mathrm{d},1}(\theta_1-\theta_2) + k_{\mathrm{d},2}\theta_2 \tag{8}$$

In this section, we present a modified Polanyi-Wigner equation for all three cases given that the energy difference between the layer is sufficiently high. Moreover, we derive an analytical solution for the coverages in the first and second layer in layer exchange equilibrium.

3.1 Modified Polanyi-Wigner equation

In the main text, we present a modified Polanyi-Wigner equation for the case of quasi-equilibrium layer exchange. This equation holds true given that the energy difference between the first and second layer is sufficiently high and the total coverage is smaller than one. Here, we derive a modified Polanyi-Wigner equation suitable for all three cases.

For a sufficiently high energy difference between the layers and a total coverage smaller than one only a very small fraction of particles resides in the second layer ($\theta_2 << \theta_1$). We can assume $\theta \approx \theta_1$. Another consequence of the small second layer coverage is that the time derivation of θ_2 is small as well, *i.e.*, $\frac{\mathrm{d}\theta_2}{\mathrm{d}t} \approx 0$. Hence, we can obtain an expression for θ_2 as a function of the total coverage by rearranging Eq. 7:

$$\theta_2 \approx \frac{2k_{\mathrm{le},1\to2}\theta^2}{2k_{\mathrm{le},2\to1}(1-\theta)+k_{\mathrm{d},2}} \tag{9}$$

Insertion of Eq. 9 into the total desorption rate (Eq. 8) yields Eq. 10. It describes the total desorption rate as a function of the total coverage for all three cases given that only a small fraction of particles resides in the second layer. As discussed for the modified Polanyi-Wigner equation presented in the main text, Eq. 10 reveals two contributions to the total desorption rate. We assign the first contribution of $k_{\mathrm{d},1}\theta$ to desorption from the first layer. The second contribution of $k_{\mathrm{d},2}\frac{2k_{\mathrm{le},1\to2}\theta^2}{2k_{\mathrm{le},2\to1}(1-\theta)+k_{\mathrm{d},2}}$ describes desorption via *hop on top* as explained in the main text.

$$\frac{r_\mathrm{d}}{N_\mathrm{ad}} \approx k_{\mathrm{d},1}\theta + k_{\mathrm{d},2}\frac{2k_{\mathrm{le},1\to2}\theta^2}{2k_{\mathrm{le},2\to1}(1-\theta)+k_{\mathrm{d},2}} \tag{10}$$

Moreover it is important to note that Eq. 10 only depends on the total coverage and model parameters and not on the first- and second-layer coverages. In contrast to the layer coverages, it is easy to calculate the total coverage from a measured desorption spectrum. Hence, we expect that the use of Eq. 10 rather than the model differential equation system can be useful for the evaluation of experimental data. For example, we expect that Eq. 10 can be fitted to a set of experimental desorption spectra in order to derive the kinetic parameters of desorption and layer exchange. This analysis strategy should, in principle, work for all three cases as it accounts for the full model kinetics. Thus, it can also be used to verify the choice of case.

In order to show that Eq. 10 is consistent with our previous findings, we show that Eq. 10 simplifies to the (modified) Polanyi-Wigner equation for case (a) (case (c)).

Case (a): kinetically-hindered layer exchange In case (a) the barrier for layer exchange is sufficiently higher than for desorption, which corresponds to $k_{\mathrm{d},2} >> k_{\mathrm{le},2\to1}$ and $k_{\mathrm{d},1} >> k_{\mathrm{le},1\to2}$ in terms of rate constants. As a consequence, we can assume $2k_{\mathrm{le},2\to1}(1-\theta)+k_{\mathrm{d},2} \approx k_{\mathrm{d},2}$ and $k_{\mathrm{d},1}+2k_{\mathrm{le},1\to2}\theta \approx k_{\mathrm{d},1}$. Next, we apply these assumption to Eq. 10, which yields Eq. 11 as an approximate total desorption rate. From Eq. 11 it is evident that only desorption from the first layer contributes in case (a). This finding is identical to our previous findings for case (a) as presented in the main text.

$$\frac{r_\mathrm{d}}{N_\mathrm{ad}} \approx k_{\mathrm{d},1}\theta + 2k_{\mathrm{le},1\to2}\theta^2 \approx k_{\mathrm{d},1}\theta \tag{11}$$

Case (c): quasi-equilibrium layer exchange Quasi-equilibrium layer exchange is characterized by a significantly higher rate of layer exchange than desorption. Hence, the relation between the rate constants is $k_{\mathrm{d},2} << k_{\mathrm{le},2\to1}$. From there we conclude $2k_{\mathrm{le},2\to1}(1-\theta)+k_{\mathrm{d},2} \approx 2k_{\mathrm{le},2\to1}(1-\theta)$, which yields Eq. 12 when applied to Eq. 10. Eq. 12 is identical with the modified Polanyi-Wigner equation derived previously.

$$\frac{r_\mathrm{d}}{N_\mathrm{ad}} \approx k_{\mathrm{d},1}\theta + k_{\mathrm{d},2}\frac{2k_{\mathrm{le},1\to2}\theta^2}{2k_{\mathrm{le},2\to1}(1-\theta)} = k_{\mathrm{d},1}\left(\theta + \frac{\theta^2}{1-\theta}\right) \tag{12}$$

3.2 Analytical solution for layer exchange equilibrium

As explained in our manuscript and section 6.3, we use the layer-exchange equilibrium layer coverages for the calculation of desorption spectra in case of quasi-equilibrium layer exchange. To this end, the equilibrium coverage distribution is calculated numerically. For the simple chain geometry, however, an analytical solution for the equilibrium layer distribution exist. We present this analytical solution in the following.

In layer exchange equilibrium the net layer exchange rate is zero. This additional condition introduces a dependence between the layer coverages, so we can express the first- and second-layer coverage as a function of the total coverage. In order to do so we write the net layer exchange rate as a function of θ_2 and θ:

$$\frac{r_\mathrm{le}}{N_\mathrm{ad}} = -2(4k_{\mathrm{le},1\to2}-k_{\mathrm{le},2\to1})\theta_2^2 + 2\left((4k_{\mathrm{le},1\to2}-k_{\mathrm{le},2\to1})\theta + k_{\mathrm{le},2\to1}\right)\theta_2 - 2k_{\mathrm{le},1\to2}\theta^2 \tag{13}$$

Next, we solve the quadric equation $\frac{r_{\mathrm{le}}}{N_{\mathrm{ad}}}(\theta_2) = 0$ and select the physical solution in order to obtain $\theta_2(\theta)$. The first layer coverage θ_1 can be calculated from the balance equation $\theta = \theta_1 + \theta_2$.

$$\theta_2 = \begin{cases} \frac{1}{2}\left(\theta + \frac{k_{\mathrm{le},2\to1}}{4k_{\mathrm{le},1\to2}-k_{\mathrm{le},2\to1}}\right) + \sqrt{\frac{1}{4}\left(\theta + \frac{k_{\mathrm{le},2\to1}}{4k_{\mathrm{le},1\to2}-k_{\mathrm{le},2\to1}}\right)^2 - \frac{k_{\mathrm{le},1\to2}}{4k_{\mathrm{le},1\to2}-k_{\mathrm{le},2\to1}}\theta^2}, & \text{for } 4k_{\mathrm{le},1\to2} < k_{\mathrm{le},2\to1} \\ \frac{1}{4}\theta^2, & \text{for } 4k_{\mathrm{le},1\to2} = k_{\mathrm{le},2\to1} \\ \frac{1}{2}\left(\theta + \frac{k_{\mathrm{le},2\to1}}{4k_{\mathrm{le},1\to2}-k_{\mathrm{le},2\to1}}\right) - \sqrt{\frac{1}{4}\left(\theta + \frac{k_{\mathrm{le},2\to1}}{4k_{\mathrm{le},1\to2}-k_{\mathrm{le},2\to1}}\right)^2 - \frac{k_{\mathrm{le},1\to2}}{4k_{\mathrm{le},1\to2}-k_{\mathrm{le},2\to1}}\theta^2}, & \text{for } 4k_{\mathrm{le},1\to2} > k_{\mathrm{le},2\to1} \end{cases} \tag{14}$$

4 Shifted chain geometry

As discussed before we consider a simple geometry in our manuscript to show the general influence of layer exchange on the kinetics of desorption. However, we expect that the model geometry influences desorption *via hop on top*, because the model differential equations depend on geometry-specific aspects like the expected number of adsorption sites in the second layer (see derivation in section 2 of our manuscript). In this section, we consider an additional geometry, in order to investigate if the model geometry does indeed influence the effect of layer exchange on desorption.

4.1 Kinetic model

In addition to the simple chain geometry presented in our manuscript, we consider a second geometry we refer to as shifted chain geometry. In the shifted chain geometry, the particles in the first layer form one-dimensional chains just like the simple chain geometry. The adsorption sites in the second layer, however, are not directly on top of particles in the first layer, but shifted half a particle diameter as shown in Fig. S7. As a consequence, every adsorption site in the second layer has two occupied adsorption sites underneath rather than one. All other model assumptions and the involved processes stay the same. The effect of this geometry change will be discussed in the following.

Diffusion For the simple chain geometry we assumed that diffusion within the layers is in equilibrium. This assumption (and its motivation) stays the same for the shifted chain geometry. Hence, we can once again assume that the particles are placed randomly on the surface. However, the occupation probabilities for the second layer change as each adsorption site in the second layer now requires two occupied adsorption sites underneath. For the shifted chain geometry the expected number of unoccupied adsorption sites in the second layer is $N_{\mathrm{ad}}\theta_1^2$ and the expected probability for an adsorption site in the second layer to be occupied θ_2/θ_1^2. Consequently, the probability for an adsorption site in the second layer to be unoccupied reads as $1 - \theta_2/\theta_1^2$.

Layer exchange To determine the net layer exchange rate for the shifted chain geometry we need to consider the relevant precursor states for layer exchange from the first (second) to the second (first) layer. Layer exchange from the first to the second layer requires a free particle in the first layer (*i.e.*, a particle with no particles on top) next to an unoccupied adsorption site in the second layer. These conditions are only fulfilled by the two configurations shown in Fig. S8 (a) (expected probability $2\theta_1^3(1-\theta_1)\left(1-\theta_2/\theta_1^2\right)^2$) and (b) (expected probability $2\theta_1^4\left(1-\theta_2\theta_1^2\right)^3$). Thus, the rate of layer exchange from the first to the second layer is $2k_{\mathrm{le},1\to2}\theta_1^2(\theta_1-\theta_2)\left(1-\theta_2/\theta_1^2\right)^2$.

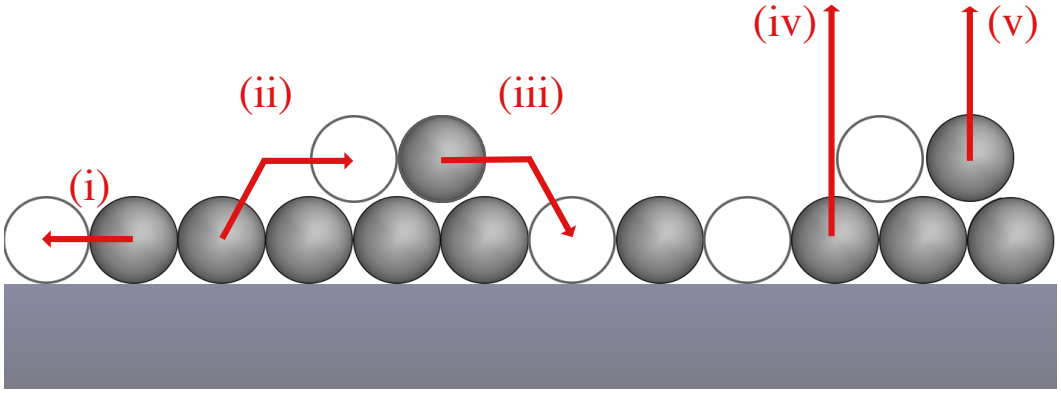

Figure S7: Schematic representation of the shifted chain geometry and elementary processes. The displayed processes are diffusion (i), layer exchange from the first to the second (ii) and from the second to the first layer (iii) as well as desorption from the first (iv) and second (v) layer. Occupied adsorption sites are displayed as filled spheres, while unoccupied adsorption sites are shown as empty spheres.

Layer exchange from the second to the first layer can only take place if a particle in the second layer is adjacent to an unoccupied adsorption site in the first layer. This requirement corresponds to the configuration shown in Fig. S8 (c) (expected probability $2(1-\theta_1)\theta_2$), so the rate for layer exchange from the second to the first layer reads as $2k_{\mathrm{le},2\to1}(1-\theta_1)\theta_2$. Consequently, the net layer exchange rate for the first layer is given by Eq. 15.

$$\frac{r_{\mathrm{le}}}{N_{\mathrm{ad}}} = -2k_{\mathrm{le},1\to2}\theta_1^2(\theta_1-\theta_2)\left(1-\frac{\theta_2}{\theta_1^2}\right)^2 + 2k_{\mathrm{le},2\to1}(1-\theta_1)\theta_2 \tag{15}$$

Desorption We model desorption from the first and second layer with a first order Polanyi-Wigner approach, respectively, as explained for the simple chain geometry in our manuscript. Again, particles in the first layer can only desorb if they are not hindered by particles in the second layer. Hence, first-layer desorption can only occur from three configurations as shown in Fig. S8 (d) (expected probability $2\theta_1(1-\theta_1)^2$), Fig. S8 (e) (expected probability $2\theta_1^2(1-\theta_1)\left(1-\theta_2/\theta_1^2\right)$) and Fig. S8 (f) (expected probability $2\theta_1^3\left(1-\theta_2/\theta_1^2\right)^2$). Consequently, the expected total probability for a free particle in the first layer is $(\theta_1-\theta_2)^2/\theta_1$ and the first-layer desorption rate reads as Eq. 16.

$$\frac{r_{\mathrm{d},1}}{N_{\mathrm{ad}}} = k_{\mathrm{d},1}\frac{(\theta_1-\theta_2)^2}{\theta_1} \tag{16}$$

As discussed before desorption from the second layer can always take place as long as there are particles in the second layer. Thus, the second-layer desorption rate is not (directly) effected by the geometry and reads as Eq. 17.

$$\frac{r_{\mathrm{d},2}}{N_{\mathrm{ad}}} = k_{\mathrm{d},2}\theta_2 \tag{17}$$

When combining the rates of layer exchange and desorption, we obtain Eq. 18 and Eq. 19 for the model differential equations.

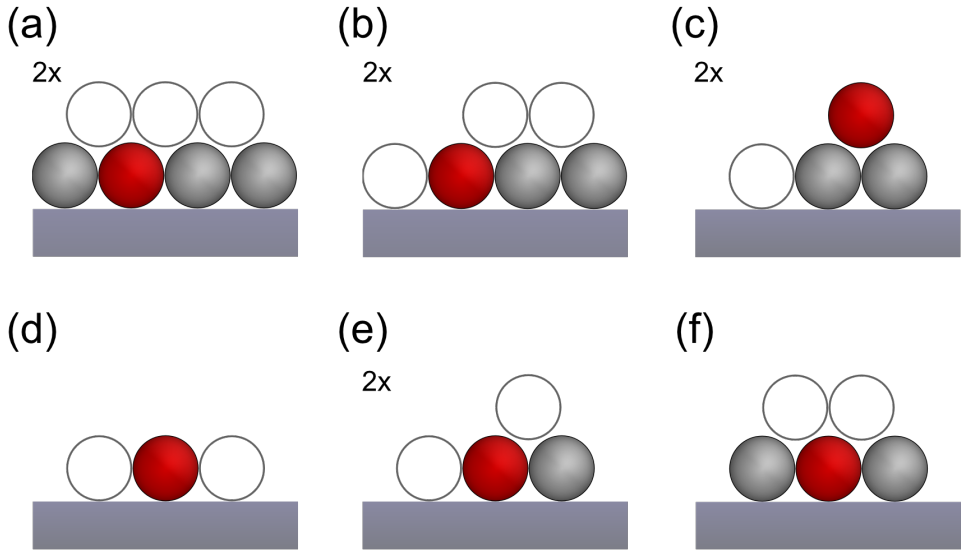

Figure S8: Schematic representation of precursor states for the involved processes in the shifted chain geometry. Particles moving in the course of the corresponding process are displayed as red spheres, stationary particles as grey spheres. Unoccupied adsorption sites are displayed as unfilled grey spheres. The figure shows the precursor states of layer exchange from the first to the second layer (a and b), layer exchange from the second to the first layer (c) and for desorption from the first layer (d-f). Precursor states (a), (b), (c) and (e) include the displayed configuration as well as the corresponding mirror image which is why they are marked with "2x".

$$\frac{\mathrm{d}\theta_1}{\mathrm{d}t} = -2k_{\mathrm{le},1\to2}\theta_1^2(\theta_1-\theta_2)\left(1-\frac{\theta_2}{\theta_1^2}\right)^2 + 2k_{\mathrm{le},2\to1}(1-\theta_1)\theta_2 - k_{\mathrm{d},1}\frac{(\theta_1-\theta_2)^2}{\theta_1} \tag{18}$$

$$\frac{\mathrm{d}\theta_2}{\mathrm{d}t} = 2k_{\mathrm{le},1\to2}\theta_1^2(\theta_1-\theta_2)\left(1-\frac{\theta_2}{\theta_1^2}\right)^2 - 2k_{\mathrm{le},2\to1}(1-\theta_1)\theta_2 - k_{\mathrm{d},2}\theta_2 \tag{19}$$

The total desorption rate (*i.e.*, the sum of the first-layer (Eq. 16) and second-layer desorption rate (Eq. 19)) for the shifted chain geometry reads as Eq. 20.

$$\frac{r_\mathrm{d}}{N_\mathrm{ad}} = k_{\mathrm{d},1}\frac{(\theta_1-\theta_2)^2}{\theta_1} + k_{\mathrm{d},2}\theta_2 \tag{20}$$

We show simulated desorption spectra for the shifted chain geometry in case of quasi-equilibrium layer exchange at varying initial coverages in section 5. Moreover, the interactive visualisation (see section 6) provided with this ESI can be used to investigate the influence of second-layer desorption and layer exchange for the shifted chain geometry. Briefly, the desorption spectra show the same three cases and characteristic features as observed for the simple chain geometry. However, the effect of second-layer desorption is always smaller for the shifted chain geometry than for the

simple chain geometry. This smaller contribution of second-layer desorption is caused by the fact that in the shifted chain geometry every second-layer adsorption site requires two occupied adsorption sites underneath while it is only one for the simple chain geometry. Thus, the number of adsorption sites in the second layer at a given coverage is always smaller for the shifted than for the simple chain geometry.

4.2 Modified Polanyi-Wigner equation

For the simple chain geometry, we considered a case where only a very small fraction of particles resides in the second layer. These considerations lead to a modified Polanyi-Wigner for second layer desorption as shown in section 3.1. When applying the same strategy to the shifted chain geometry, we obtain a different modified Polanyi-Wigner (Eq. 21). Comparison of the modified Polanyi-Wigner equations of the simple and shifted chain geometries (Eq. 21 and Eq. 22) shows that both equations are very similar. However, the equations differ in the exponent of the coverage in the contribution of second layer desorption (θ^2 for the simple chain and θ^3 for the shifted chain). This finding supports our expectation that the influence of desorption *via hop on top* depends on the adsorption geometry. Moreover, we conclude that the contribution of second-layer desorption is smaller for the shifted chain geometry than for the simple chain geometry, because $\theta^3 < \theta^2$ for $\theta < 1.0\,\mathrm{ML}$.

$$\frac{r_\mathrm{d}}{N_\mathrm{ad}} \approx k_{\mathrm{d},1}\theta + k_{\mathrm{d},2}\frac{2k_{\mathrm{le},1\to2}\theta^3}{2k_{\mathrm{le},2\to1}(1-\theta)+k_{\mathrm{d},2}} \tag{21}$$

In case of quasi-equilibrium layer exchange Eq. 21 simplifies to Eq. 22.

$$\frac{r_\mathrm{d}}{N_\mathrm{ad}} \approx k_{\mathrm{d},1}\theta + k_{\mathrm{d},2}\frac{2k_{\mathrm{le},1\to2}\theta^3}{2k_{\mathrm{le},2\to1}(1-\theta)} = k_{\mathrm{d},1}\left(\theta + \frac{\theta^3}{1-\theta}\right) \tag{22}$$

5 Contribution of desorption via *hop on top* depending on initial coverage and geometry

Next, we analyse the effect of layer geometry and initial coverage on desorption *via* the *hop on top* mechanism. To this end, we consider the case of quasi-equilibrium layer exchange (case (c)), because case (c) serves as an upper limit for the contribution of desorption *via hop on top* to submonolayer desorption.[†]

Desorption spectra In order to elucidate the coverage and geometry dependence of desorption *via hop on top*, we present a set of desorption spectra for each geometry in Fig. S9 (a). Both sets of desorption spectra were calculated based on the same kinetic parameters we use in our manuscript (see explanation in our manuscript or Tab. 1) and initial coverages between 0.1 ML and 1.0 ML in steps of 0.15 ML. Fig. S9 (a) shows that desorption spectra with the same initial coverage are similar for both geometries (high and low opacity curves in Fig. S9 (a)). Especially, both geometries reveal desorption spectra with the same characteristic features discussed for case (c) in our manuscript (a single asymmetric peak with a higher peak width and more pronounced low temperature rise

[†]We consider only systems with a high energy difference between the first and second layer. Therefore, the second layer is depopulated by desorption before the system reaches temperatures where desorption from the first layer becomes relevant. The second-layer occupation relevant for desorption *via hop on top*, however, is solely created by layer exchange and, thus, is always smaller or equal to the equilibrium second-layer occupation. As a consequence, the contribution of desorption *via hop on top* is maximum in case of layer exchange equilibrium.

than a first-order Polanyi-Wigner peak). However, these features are barely noticeable for small coverages and become more pronounced with increasing coverage (compare the red and blue curve in Fig. S9 (a)). For an initial coverage of 1.0 ML the features caused by second-layer desorption are developed the most. Hence, this findings confirm our expectation that the contribution of second-layer desorption increases with coverage as discussed in our manuscript.

Concerning geometry, the differences between desorption spectra with the same initial coverage but a different geometry are small as can be seen in Fig. S9. For small coverages Fig. S9 (a) shows that the desorption spectra of both geometries are nearly identical (red curves). With increasing coverage, however, the peaks of both geometries are increasingly different. The desorption signal of the simple chain geometry have a higher peak width and smaller maximum desorption rate as the shifted chain desorption signal. Moreover the total shift in the peak maxima is smaller for the shifted chain geometry than for the simple chain geometry. As these features are characteristic for the contribution of second-layer desorption, this confirms our conclusion that desorption *via hop on top* contributes more for the simple chain geometry than for the shifted chain geometry (see section 4.2).

Contribution of the *i*th layer To quantify the influence of desorption *via hop on top* we consider the contribution of the ith layer χ_i (Eq. 23). This quantity describes the fraction of particles desorbing from the i^{th} layer relative to all particles desorbing in a given peak. Thus, for the submonolayer desorption peak χ_1 quantifies the contribution of desorption directly from the first layer and χ_2 quantifies desorption *via hop on top*. By definition, the sum of all layer contributions is unity (*i.e.*, $\sum_i \chi_i = 1$).

$$\chi_i = \frac{\int_{\text{peak}} \mathrm{d}t r_{\mathrm{d},i}(t)}{\int_{\text{peak}} \mathrm{d}t r_{\mathrm{d}}(t)} \tag{23}$$

For both geometries discussed in this ESI, we can calculate the layer contributions in case of quasi-equilibrium layer exchange analytically. In order to do so we use $\frac{r_1}{N_{\text{ad}}} \approx k_{\mathrm{d},1}\theta$ as well as the modified Polanyi-Wigner equations derived in section 3.1 and 4.2, respectively (Eq. 12 and Eq. 22). We insert these equations in Eq. 23 and solve the integral. In doing so, we obtain Eq. 24 for χ_1 in case of the simple chain geometry and Eq. 25 in case of the shifted chain geometry. The contribution of the second layer χ_2 can be calculated by $\chi_2 = 1 - \chi_1$

$$\chi_{1,\text{simple}} = 1 - 0.5\theta \tag{24}$$

$$\chi_{1,\text{shifted}} = \frac{1}{\sqrt{3}} \tan^{-1}\left(\frac{2\theta - 1}{\sqrt{3}}\right) - 0.5 \ln\left(\theta^2 - \theta + 1\right) - \frac{1}{\sqrt{3}} \tan^{-1}\left(-\frac{1}{\sqrt{3}}\right) \tag{25}$$

In Fig. S9 (b) we present the contribution of first-layer (red) and second-layer (blue) desorption for submonolayer desorption as functions of the total peak coverage θ_{mono} for the simple chain (high opacity) and shifted-chain (low opacity) geometries. Note that the peak coverage θ_{mono} is equal to the initial coverage θ as desorption spectra in case (c) show no second-layer desorption signal for initial coverages $\theta < 1$ (see Fig. S9 (a)). Fig. S9 (b) shows that second-layer desorption does not contribute in the limit of zero coverage independent of the geometry. However, with increasing coverage the contribution of second-layer desorption increases and reaches its maximum when the first layer is fully occupied ($\theta_{mono} = 1.0$ ML). The maximum contribution of second-layer desorption for the simple chain (shifted-chain) geometry is $\chi_{2,\text{simple}} = 0.50$ ($\chi_{2,\text{shifted}} \approx 0.40$), *i.e.*, 50% (40%) of the particles residing in the first layer desorb *via* the second layer. Moreover, Fig. S9

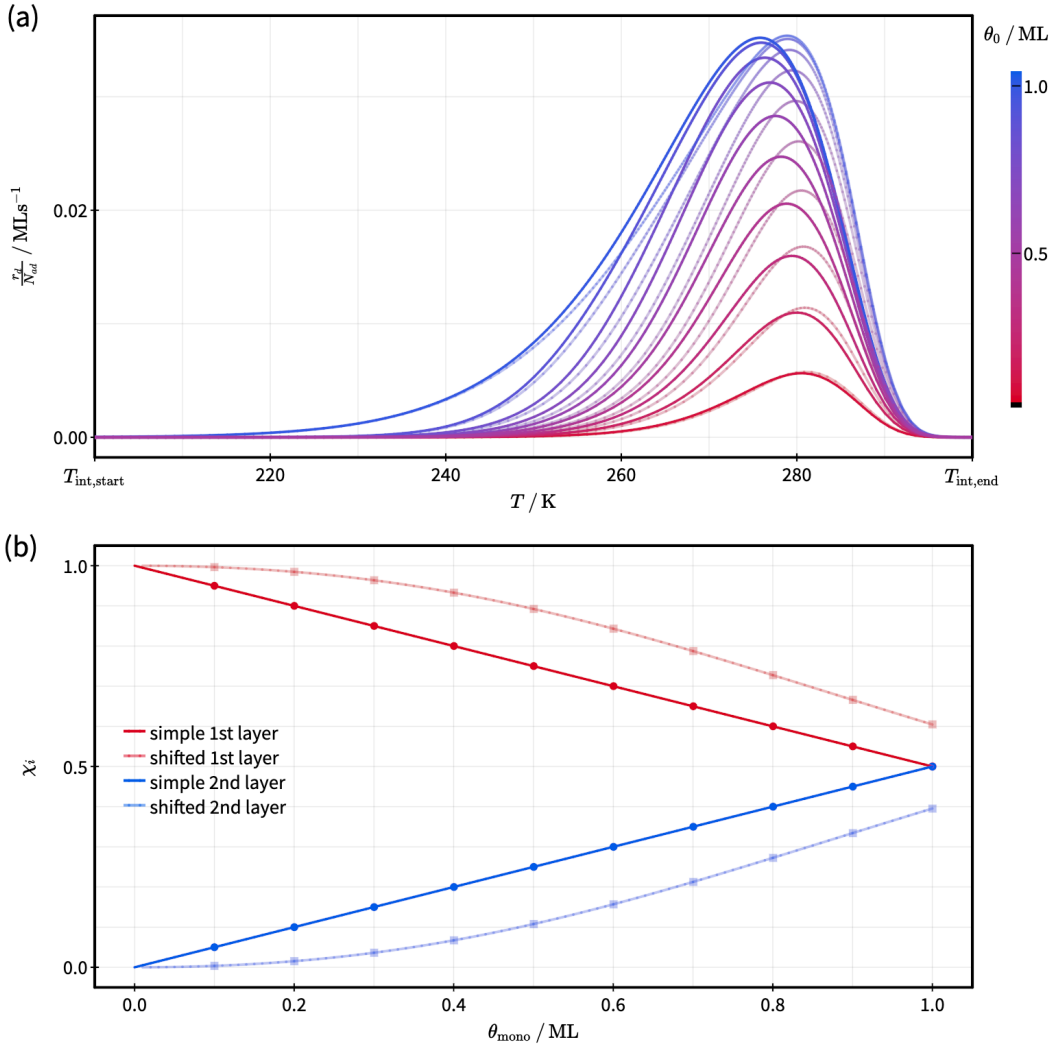

Figure S9: Comparison of the simple chain and shifted chain geometries. Results for the simple (shifted) chain geometry are displayed with high (low) opacity. (a) Set of desorption spectra with different initial coverages θ_0 calculated for a two-layer system according to our model. (b) Contribution χ_i for first-layer (second-layer) desorption as a function of the total integral over the monolayer desorption signal in red (blue). The analytical solutions are displayed as lines and numerical values calculated for the simulated desorption spectra in (a) are displayed as points. The temperatures $T_{\mathrm{int,start}}$ and $T_{\mathrm{int,end}}$ in (a) are the limits used for peak integration in order to calculate the contributions displayed in (b).

(b) shows that the contribution of second-layer desorption is always smaller in case of the shifted chain geometry compared to the simple chain geometry. As discussed before, this smaller contribution of second-layer desorption is caused by a lower number of adsorption sites in the second

layer for the shifted chain geometry compared to the simple chain geometry ($\theta_1^2 \leq \theta_1$) (see section 4.1). We conclude that the contribution of second-layer desorption decreases with the number of adsorption sites in the second layer.

6 Calculation of desorption spectra

In this section, we provide details concerning the calculation of desorption spectra from the model equations derived in the main text, *e.g.*, the calculation of initial coverages and the numerical solution of layer exchange equilibrium. The complete javascript code used for our calculations is published online as an interactive visualisation (https://doi.org/10.4119/unibi/2955951).

6.1 Initial coverages: ballistic model for dosing

In case of quasi-equilibrium layer exchange the initial coverage distribution prepared by dosing does not influence the desorption spectrum as the system enters its equilibrium state prior to desorption. For a kinetically-hindered layer exchange, however, the initial first- and second-layer coverages have a significant influence on the observed desorption spectra as shown in section 2.2. Consequently, it is necessary to derive a realistic initial coverage distribution to analyse the implications of a kinetically-hindered layer exchange. To this end, we develop a simple ballistic model for dosing to understand the general influence of dosing on the appearance of desorption spectra. We do not intent to describe special dosing scenarios (*e.g.*, dosing with high kinetic energies in a molecular beam) with this simple ballistic model.

Our model is based on the assumption that particles are hitting the sample surface randomly with a given collision rate. All particles colliding with an unoccupied adsorption site (in the first or second layer) stick to the surface with a certain probability while particles colliding with an occupied adsorption site do not adsorb. Thereby, we describe both, collision rate and sticking probability, in terms of one effective flux f as a function of time t. Furthermore, we assume that the sticking coefficients for the first and second layer are equal, because we expect this to be the case for low temperatures where close to all colliding particles stick. For higher temperatures, however, this assumption might not be suitable.

Moreover, we consider a case where particles do not leave the layer they initially adsorbed to. This choice is motivated by the procedure of a typical TPD experiment and the intended application of the dosing model to cases (b) and (c). In a typical TPD experiment, particles are deposited onto a sample surface kept at temperatures much lower than the desorption temperature in order to prevent desorption prior to the actual experiment. As we consider cases where the rates of layer exchange are comparable to or smaller than the desorption rate at the desorption temperature, we conclude that layer exchange is not activated at the temperature of particle deposition.

Please note that our ballistic model is not applicable when the barrier for layer exchange is sufficiently low resulting in layer exchange during dosing. In that case, however, we can assume that layer exchange is significantly faster than desorption, because desorption — in contrast to layer exchange — does not take place during dosing. Thus, we can calculate the coverage distribution without a model for dosing by solving the equilibrium condition for layer exchange (see section 6.3).

In case of the simple chain geometry discussed in the main text the model assumptions presented above translate into Eq. 26 and Eq. 27 for the adsorption rates in the first and second layer $\frac{r_{\mathrm{ad},1}}{N_{\mathrm{ad}}}$ and $\frac{r_{\mathrm{ad},2}}{N_{\mathrm{ad}}}$, respectively. The total adsorption rate $\frac{r_{\mathrm{ad}}}{N_{\mathrm{ad}}}$ is given by Eq. 28.

$$\frac{r_{\mathrm{ad},1}}{N_{\mathrm{ad}}} = \frac{\mathrm{d}\theta_1}{\mathrm{d}t} = f(t)(1-\theta_1) \tag{26}$$

$$\frac{r_{\mathrm{ad},2}}{N_{\mathrm{ad}}} = \frac{\mathrm{d}\theta_2}{\mathrm{d}t} = f(t)(\theta_1-\theta_2) \tag{27}$$

$$\frac{r_{\mathrm{ad}}}{N_{\mathrm{ad}}} = \frac{\mathrm{d}\theta}{\mathrm{d}t} = f(t)(1-\theta_2) \tag{28}$$

The derived inhomogeneous differential equations for the first- and second-layer coverages (Eq. 26 and Eq. 27) form a coupled differential equation system, where Eq. 27 depends on θ_1 and θ_2, but Eq. 26 only depends on θ_1. Therefore, we can first solve Eq. 26 independently and then use the solution to solve Eq.27. This yields Eq. 29 and Eq. 30 for the coverages in the first and second layer as a function of time, respectively, where $F(t)$ is the accumulated effective flux as defined by Eq. 31.

$$\theta_1(t) = 1 - \mathrm{e}^{-F(t)} \tag{29}$$

$$\theta_2(t) = 1 - (1+F(t))\mathrm{e}^{-F(t)} \tag{30}$$

$$F(t) = \int_0^t d\tau f(\tau) \tag{31}$$

The total coverage as a function of time reads as Eq. 32.

$$\theta(t) = 2 - (2+F(t))\mathrm{e}^{-F(t)} \tag{32}$$

Eq. 29 and Eq. 30 can be used to calculate the initial coverage distribution as a function of the accumulated flux. For the calculation of theoretical desorption spectra, however, it is more useful to express the (initial) first- and second-layer coverages as a function of the dosed total coverage θ instead of the accumulated flux $F(t)$. Hence, we inverted Eq. 32 which yields Eq. 33 for the total coverage as a function of the accumulated flux, where W is the product logarithm function (or Lambert W function). We can use Eq. 33 to calculate the accumulated flux corresponding to each total coverage, which, in turn, can be used to calculate the wanted initial coverage distribution.

$$F(t) = 2 - W((\theta-2)\mathrm{e}^{-2}) \tag{33}$$

Fig. S10 shows the first- and second-layer coverages calculated with our ballistic model as functions of the accumulated flux (a) and the total coverage (b). In terms of accumulated flux the rise in total coverage (black) is largely identical with the increase of the first-layer coverage (red) for very small $F(t)$ (S10 (a)). With increasing accumulated flux (and total coverage), however, the number of unoccupied adsorption sites in the first layer decreases, while unoccupied adsorption sites in the second layer are created. Hence, more and more particles adsorb in the second layer, which leads to a significant second-layer coverage. For example at a dosed total coverage of 0.5 ML the coverages of the first and second layer are approximately 0.4 ML and 0.1 ML, which means that 20 % of the particles on the surface reside in the second layer. We conclude that — as part of our ballistic model — adsorption does not happen layer by layer, but the first and second layer are simultaneously. As a consequence, we expect the kinetics of dosing to have a great impact on the desorption spectra of systems where layer exchange is kinetically-hindered (*i.e.*, particles cannot leave the layer they adsorbed to).

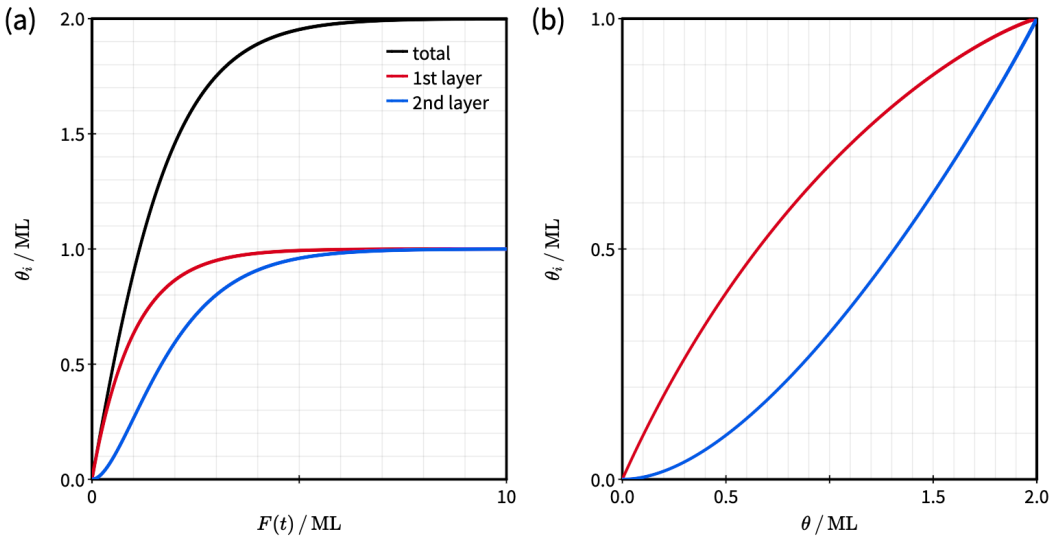

Figure S10: Coverages in the first (red) and second (blue) layer as calculated by our ballistic model. The coverages are shown as functions of the accumulated effective flux $F(t)$ (a) and the total coverage θ (b). The total coverage as a function of the accumulated flux (black) is shown in (a).

6.2 Numerical integration of the full differential equation system

Desorption spectra were calculated numerically from a given set of initial coverages and kinetic parameters. To this end, the first- and second-layer coverages as a function of time (or temperature) were calculated by numerical integration of Eq. 6 and Eq. 7 with a fourth order Runge-Kutta algorithm. Desorption rates were calculated from the coverages with Eq. 8. As part of this calculation we altered the standard Runge-Kutta algorithm by making the step size variable with the rates of the involved processes. The step size Δt was determined by the timescale of the fastest process as shown in Eq. 34. We base the definition of a process' timescale on the lifetime of a first order process $\tau = 1/k = r/\theta$. Additionally, we introduced a prefactor of 0.01, which means that we calculate 100 points per lifetime of the fastest process (the choice of exactly 100 points is arbitrary). To limit the maximum calculation time and prevent missing relevant features we chose time step limits of $\Delta t_{\mathrm{min}} = 1 \times 10^{-6}$ s and $\Delta t_{\mathrm{max}} = 1$ s.

$$\Delta t = 0.01 \min\left(\frac{\theta_1 N_{\mathrm{ad}}}{r_{\mathrm{d},1}}, \frac{\theta_2 N_{\mathrm{ad}}}{r_{\mathrm{d},2}}, \frac{\theta_1 N_{\mathrm{ad}}}{r_{\mathrm{le},1\to2}}, \frac{\theta_2 N_{\mathrm{ad}}}{r_{\mathrm{le},2\to1}}\right) \tag{34}$$

6.3 Numerical integration procedure in case of quasi-equilibrium layer exchange

We discussed before in the main text that a normal Runge-Kutta algorithm reaches its limitations in terms of computation time for small barriers of layer exchange. Given that the barrier of layer exchange is very small compared to the desorption barrier, the rates of layer exchange are magnitudes higher than the desorption rate. Hence, an accurate numeric integration requires very small time steps on the timescale of a TPD experiment. This time step, in turn, increases the computation time drastically. While long computation times might not be a problem when working with

very powerful computers, standard personal computers will reach their limits easily. These limits are especially relevant for the calculation of multiple desorption spectra or future applications like the fitting of measurement data. However, the calculation only becomes computationally intensive when layer exchange is magnitudes faster than desorption. Thus, this problem with computation power is only relevant for systems where case (c), quasi-equilibrium layer exchange, is applicable (see section 2.1). As a consequence, we can treat layer exchange implicitly by calculation of the first- and second-layer coverages from the total coverage rather than solving the full differential equation system. This way we can decrease the computing effort significantly as will be explained in the following.

If the system is in a state of quasi-equilibrium layer exchange on the timescale of desorption the net-layer exchange rate (Eq. 35) is zero (except for a small time interval directly after desorption of a particle). This condition creates a relation between the coverages of the first and second layer. Hence, we can express the layer coverages as functions of the total coverage θ by solving $\frac{r_{\mathrm{LE}}}{N_{\mathrm{ad}}} = 0$. In order to do so, we rewrite Eq. 35 as a function of the total coverage and the second-layer coverage by using the coverage balance $\theta_1 = \theta - \theta_2$ (see Eq. 36). From there we calculate the zero of Eq. 36 numerically[‡] with a Newton-Raphson algorithm to obtain the second-layer coverage in case of equilibrium. The coverage of the first layer can be calculated from θ and θ_2 with the coverage balance.

$$\frac{r_{\mathrm{le}}}{N_{\mathrm{ad}}}(\theta_1, \theta_2) = -2k_{\mathrm{le},1\to2}(\theta_1 - \theta_2)^2 + 2k_{\mathrm{le},2\to1}(1 - \theta_1)\theta_2 \tag{35}$$

$$\frac{r_{\mathrm{le}}}{N_{\mathrm{ad}}}(\theta, \theta_2) = -2k_{\mathrm{le},1\to2}(\theta - 2\theta_2)^2 + 2k_{\mathrm{le},2\to1}(1 - \theta + \theta_2)\theta_2 \tag{36}$$

Next, we apply the equilibrium condition on the model differential equations 6 and 7. This leads to the much simpler Eq. 37. Here, it is important to note two things: First, Eq. 37 only depends on one variable as θ_1 and θ_2 are expressed as functions of the total coverage, and second, the rates of layer exchange are not part of Eq. 37 because they do not change the total coverage. As a consequence, the time step for the numerical integration of Eq. 37 only depends on the desorption rate and not on the rates of layer exchange. Hence, a large difference in the rates of layer exchange and desorption does not lead to problems with the computational effort any more. Instead, we need to solve Eq. 36 for every calculated point in order to determine the layer coverages. In practical applications, however, it is much faster to find the zero of Eq. 36 for a bigger time step than integrating the full differential equation system (Eq. 6 and Eq. 7) with a very small time step. As a consequence, this calculation strategy based on the equilibrium layer coverages solves the issues with computation time in case of low barriers for layer exchange. These explanations can be verified by comparing the simulation algorithms in the interactive visualisation published with this work (see section 6).

$$\frac{\mathrm{d}\theta}{\mathrm{d}t} = k_{\mathrm{d},1}\theta_1(\theta) + (k_{\mathrm{d},2} - k_{\mathrm{d},1})\theta_2(\theta) \tag{37}$$

We confirm that the proposed simplified simulation algorithm does indeed yield the same results as the full simulation in case of layer exchange equilibrium (case (c)). In order to do so, we carried out calculations with the full differential equation system for the limiting parameter set between cases (c) and (b) (cyan line in Fig. S3) for a minimal time step of 1×10^{-8} s. The results of

[‡]For the simple chain geometry an analytical solution of Eq. 36 exists as well (see section 3.2).

these calculations show excellent agreement with calculations relying on the layer exchange equilibrium algorithm, so we expect the calculations with the layer exchange equilibrium algorithm yield excellent results as long as case (c) applies.

References

[1] S. R. Kachel, B. P. Klein, J. M. Morbec, M. Schoniger, M. Hutter, M. Schmid, P. Kratzer, B. Meyer, R. Tonner and J. M. Gottfried, *Journal of Physical Chemistry C*, 2020, **124**, 8257–8268.